Chemical Geology 648 (2024) 121953

Contents lists available at ScienceDirect

Chemical Geology

journal homepage: www.elsevier.com/locate/chemgeo

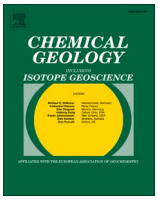

Constraining uncertainty in boron isotope systematics using a Bayesian inversion engine reveals contrasting parameter sensitivities

Aled D. Evans *, Gavin L. Foster, Damon A.H. Teagle

School of Ocean and Earth Science, National Oceanography Centre Southampton, University of Southampton, Southampton SO14 3ZH, UK

ARTICLE INFO

Editor: Vasileios Mavromatis

Keywords:
Boron isotopes
Serpentinization
Bayesian inversion
Fluid-rock exchange
Equilibrium isotope fractionation
Parameter estimation

ABSTRACT

Physical parameters within boron isotope systematics form a complex interplay that determine the boron isotopic composition of rocks, minerals, and fluids, but to date, providing constraints on uncertainty within boron equilibrium isotope modelling remains elusive. This underlying uncertainty limits the potency of boron isotopes as a tool for detecting fluid-rock exchange. A new equilibrium boron mineral-fluid fractionation modelling approach, named EquiB, coupled with a Bayesian inversion engine is presented, providing robust and reproducible constraints on the uncertainty of physical parameters encoded into a boron isotopic composition of a rock in equilibrium with a fluid. We demonstrate the validity of our approach by applying the model to several basalt-fluid and peridotite-fluid exchange scenarios. The model output generates multi-dimensional posterior probability distributions that show temperature is the greatest control on mineral-fluid fractionation in all applied scenarios. At high temperatures (defined as >50 °C) pH-dependent fractionation is negligible, but at low temperatures (defined as <50 °C) pH-dependent fractionation is a control on boron isotopic compositions. At geologically reasonable conditions other parameters such as salinity, fluid density, and pressure have little effect on the extent of boron mineral-fluid fractionation. Model outputs agree with experimentally derived fractionation factors at typical hydrothermal conditions but diverge at low temperatures. This approach provides robust constraints of parameter uncertainty, enabling meaningful interpretation of boron isotope analyses and the ability to fingerprint isotopic compositions with greater confidence.

1. Introduction

Boron is a powerful tracer of fluid-rock exchange in many natural and anthropogenic settings such as mid-ocean ridge hydrothermal systems, serpentinizing environments, groundwater contamination, and tracing pollutants (e.g., Barth, 1998; Harkness et al., 2018; James and Palmer, 2000; Lemarchand et al., 2000; Martin et al., 2016; Spivack and Edmond, 1987; Vengosh, 1998; Vengosh et al., 1994, 1999). The boron isotopic composition of rocks, minerals and fluids are usually presented using the common delta notation for stable isotopes (Craig, 1961), in this case, $\delta^{11}B$. The boron isotopic composition ($\delta^{11}B$) of a rock or mineral in equilibrium with a fluid is dependent on multiple physical parameters such as temperature, pH, pressure, salinity, and fluid density. However, for many natural systems these parameters are poorly constrained or unknown (e.g., Deyhle and Kopf, 2005; Palmer, 1996), resulting in significant uncertainties. Consequently, deeper interpretations of boron systematics, and hence fluid-rock interaction, by applying equilibrium isotope fractionation modelling have to date remained out of reach due to the underlying uncertainty of essential model parameters. In particular, the relative importance of differing physical parameters in determining the boron isotopic composition of a mineral in equilibrium with a fluid are generally unknown.

Boron is highly soluble resulting in an affinity for the fluid phase. The ~10% difference in the atomic mass of its stable isotopes, ^{10}B and ^{11}B, results in strong mass dependent fractionation during interactions within the Earth system (Kowalski and Wunder, 2018). These distinctive characteristics result in boron isotopes being a potent tool for detecting fluid-rock exchange in ocean crustal rocks and serpentinites with previous studies reporting a range of isotopic composition of between −12 and +40 ‰ for ocean floor rocks (Fig. 1) (e.g., Benton et al., 2001; Boschi et al., 2008; Martin et al., 2016; Smith et al., 1995; Spivack and Edmond, 1987; Vils et al., 2009). However, fingerprinting the origin of the boron isotopic composition and establishing the conditions of fluid-rock exchange has, to date, remained challenging primarily due to the inherent uncertainty of equilibrium boron mineral-fluid fractionation processes.

* Corresponding author.
E-mail address: A.Evans@soton.ac.uk (A.D. Evans).

https://doi.org/10.1016/j.chemgeo.2024.121953
Received 3 June 2023; Received in revised form 17 January 2024; Accepted 18 January 2024
Available online 28 January 2024

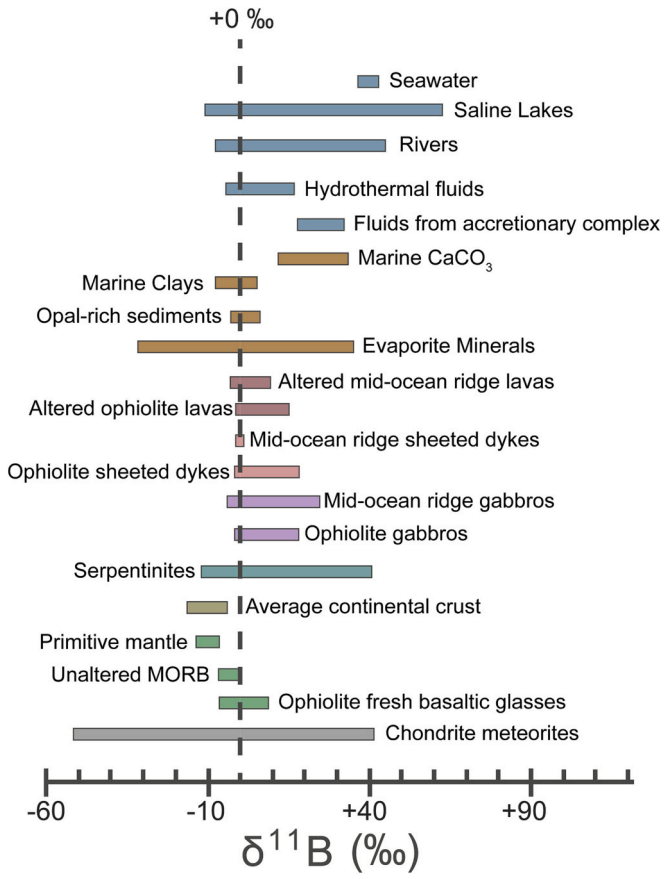

Fig. 1. Caltech plot of $\delta^{11}B$ values in nature separated by reservoir type. Adapted from Foster et al., 2016. Sources from Foster et al., 2016 and references therein.

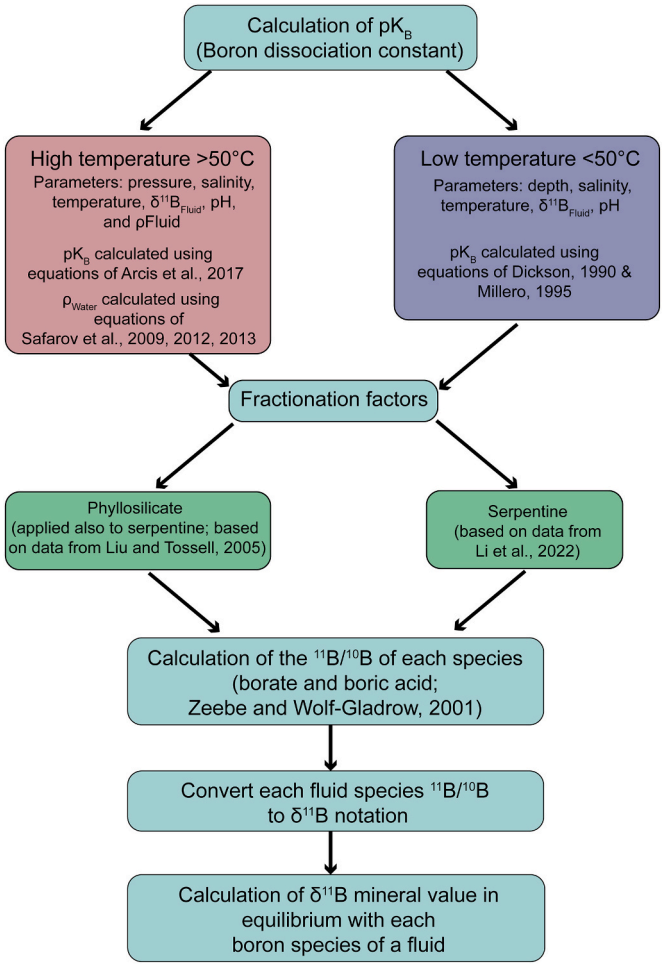

Fig. 2. EquiB model flowchart showing the various stages of the model in order to calculate a boron isotopic composition of a rock in equilibrium with a fluid.

Boron isotope fractionation between a fluid and mineral has been demonstrated to be temperature and pH-dependent, due to the pH-dependent nature of boron speciation in water (Kakihana et al., 1977; Klochko et al., 2006; Wunder et al., 2005). The relative proportion of the respective boron species in seawater defined by the boron dissociation constant (pK_B) can be calculated at a given temperature and salinity (Dickson, 1990). Boron speciation in seawater is determined by the acid-base equilibrium between boric acid and borate ion, which is dependent on pH, salinity, temperature, pressure, and fluid density (Arcis et al., 2017; Dickson, 1990; Millero, 1995; Nir et al., 2015). The boron dissociation constant in seawater (pH ~8) at surface conditions is typically ~8.6 (e.g., Dickson, 1990) resulting in significant pH-dependent isotopic fractionation and discernible changes in the relative abundance of boric acid and borate ion in seawater over the natural range of pH found on the Earth's surface.

There have been previous attempts to calculate the extent of equilibrium boron isotope fractionation between fluid and phyllosilicate or serpentine minerals using ab initio calculated fractionation factors (Li et al., 2022; Liu and Tossell, 2005), but these methods do so without considering the changing boron dissociation constant (Boschi et al., 2008; Li et al., 2022; Martin et al., 2016). This results in significant uncertainty since the fluid boron speciation, and therefore the role of pH-dependent fractionation, is unknown, which produces significant variation in calculated $\Delta^{11}B_{Mineral\text{-}Fluid}$ ($\delta^{11}B_{Mineral}$ - $\delta^{11}B_{Fluid}$) values that at 200 °C, range from −23 to −40 ‰ (Li et al., 2022). As a result, meaningful interpretation of the fluid-rock exchange processes that involve significant changes in pH is hindered. In total, these issues result in a difference of 17 ‰ at 200 °C in $\Delta^{11}B_{Mineral\text{-}Fluid}$ values between previously applied phyllosilicate-serpentine and serpentine fractionation factors with the respective boron species assumed to be proportionally equal in the fluid (Li et al., 2022; Liu and Tossell, 2005). Consequently, these previous equilibrium boron isotope fractionation models fail to robustly account for all required physical parameters that affect boron fluid-rock exchange.

To investigate the underlying uncertainty within the physical parameters involved in equilibrium boron isotope fractionation modelling we present a probabilistic modelling approach coupled with a Bayesian inversion engine to robustly constrain the uncertainty of required parameters. We document the contrasting sensitivities of individual parameters and compare the effect of using differing fractionation factors on the resulting outputs. We further demonstrate the universality of our approach and its applicability in yielding meaningful interpretations of boron isotope systematics in altered rocks.

2. EquiB: a robust and reproducible approach for equilibrium boron isotope fractionation modelling

2.1. Equilibrium boron isotope fractionation model

It is proposed that fractionation between the two B isotopes, ^{10}B and ^{11}B, is predominantly controlled by their relative portioning between the trigonal ($B(OH)_3$) and tetrahedral ($B(OH)_4^-$) species (e.g., Kowalski and Wunder, 2018). Fractionation of boron isotopes in seawater is typically expressed by the fractionation factor (Eq. (1)):

$$\alpha_{III-IV} = \frac{\frac{^{11}B}{^{10}B}trigonal}{\frac{^{11}B}{^{10}B}tetrahedral} \quad (1)$$

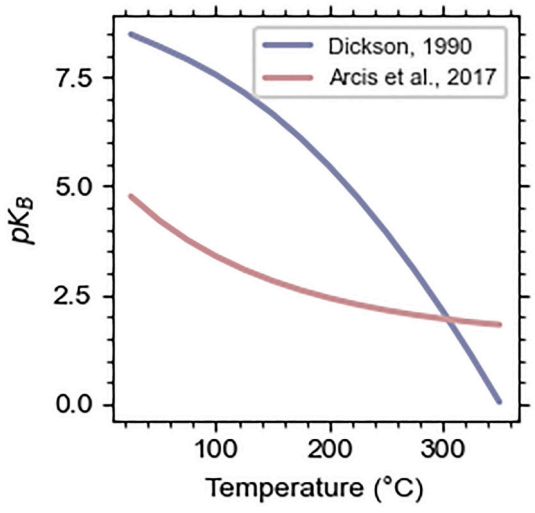

Fig. 3. Plot of calculated boron dissociation constant (pK_B) against Temperature (°C) using the high temperature (25 to 350 °C; 25 MPa; Arcis et al., 2017) and low temperature (0 to 45 °C; Dickson, 1990; 25 MPa, pressure correction Millero, 1995) approaches. The different approaches show distinct trends rather than a continuum of pK_B values.

Boron isotope compositions observed in nature vary widely from $-40\ ‰ < \delta^{11}B < +60\ ‰$ (Fig. 1), with $\delta^{11}B$ expressed through (Eq. (2)):

$$\delta^{11}B = \left(\frac{\frac{^{11}B}{^{10}B}sample}{\frac{^{11}B}{^{10}B}SRM\ 951} - 1 \right) \bullet 1000 \quad (2)$$

$^{11}B/^{10}B$ refers to the ratio of the abundances of the stable boron isotopes. The boron isotopic composition of samples are compared to National Institute of Standards and Technology (NIST) Standard Reference Material (SRM) 951 boric acid ($^{11}B/^{10}B_{SRM951} = 4.04367$; (Catanzaro, 1970). The $\delta^{11}B$ values of minerals in equilibrium with a fluid can be calculated if the distribution of borate and boric acid, pH, temperature, salinity, and pressure in the fluid are known (Fig. 2). Here we use theoretically calculated boron fractionation factors determined for phyllosilicate (mica-like; Liu and Tossell, 2005) and serpentine (Li et al., 2022). The relative partitioning between boron species can be determined if the boron dissociation constant (pK_B) is known (Fig. 3). In seawater, the relative partitioning between boron species stems from the acid-base equilibrium between boric acid and borate (Eqs. (3), (4)):

$$B(OH)_3 + H_2O \rightleftharpoons H^+ + B(OH)_4^-, \quad (3)$$

$$K_B = \frac{H^+ \bullet B(OH)_4^-}{B(OH)_3} \quad (4)$$

pK_B is a function of temperature, salinity, pH, and pressure. For low temperature (0 to 45 °C) seawater pK_B can be calculated using the following equations (Dickson, 1990; Millero, 1995) (Eqs. (5)–(7)):

$$K_B = exp\left[\frac{\left(-8966.9 - 2890.53 \bullet S^{\frac{1}{2}} - 77.942 \bullet S + 1.728 \bullet S^{\frac{3}{2}} - 0.0996 \bullet S^2 \right)}{K} + 148.0248 + 137.1942 \bullet S^{\frac{1}{2}} + 1.62142 \bullet S + \left(-24.4344 + 25.085 \bullet S^{\frac{1}{2}} + 0.2474 \bullet S \right) \bullet ln(K) + 0.053105 \bullet S^{1/2} \bullet K \right] \quad (5)$$

Table 1
Notation/symbology.

Symbol	Definition	Unit
$\delta^{11}B$	Boron isotope composition	‰
$R = \frac{^{11}B}{^{10}B}$	Boron isotope ratio	
$B(OH)_3$	Boric acid	
$B(OH)_4^-$	Borate ion	
H^+	Proton	
pK_B	Boron dissociation constant	
T	Temperature in Celsius	°C
K	Temperature in Kelvin	K
ρ_{Water}	Density of solution	kg/m^3
P	Pressure	Bar or MPa
S	Salinity	g/kg

Table 2
Coefficients for Eq. (8) from Arcis et al., 2017.

	P_1	P_2	P_3	P_4	P_5
Arcis et al., 2017	−29.2076	3359.88	9.17470	10.2855	−0.0160357

$$P_{Factor} = \left(\frac{(29.48 - 0.1622 \bullet T + 0.002608 \bullet T^2)}{83.14472 \bullet K} \right) \bullet P + 0.5 \bullet \left(\frac{0.00284}{83.14472 \bullet K} \right) \bullet P^2 \quad (6)$$

$$pK_B = exp(lnK_B + P_{Factor}) \quad (7)$$

where K is temperature in Kelvin, T is temperature in Celsius, S is salinity in g/kg, P is pressure in bars (Table 1). A different approach is required to calculate pK_B values of fluids at higher (>50 °C) temperatures following the experimental determination of boron dissociation constants (pK_B) at hydrothermal conditions (25 to 350 °C, 25 MPa (Arcis et al., 2017). The pK_B of a fluid such as modified seawater at hydrothermal conditions can be calculated through the following (Eq. (8); Fig. 3):

$$pK_B = p_1 + \frac{p_2}{K} + p_3 \bullet log(K) + (p_4 + p_5 \bullet K) \bullet log\rho_{Water} \quad (8)$$

where the respective coefficients for parameter p are reported in Table 2, K is temperature in Kelvin, and ρ_{Water} refers to the density of the solution (Table 1). The properties of seawater (pressure, density, temperature) can be calculated using an equation of state (e.g., Knudsen, 1901; Millero, 2010) that are based on experimentally derived empirical equations. Experiential studies have recently measured the properties of seawater (Safarov et al., 2009, 2012, 2013) at high temperatures (up to 200 °C), pressures (up to 140 MPa), and salinities (up to 55 g/kg), where the properties of seawater can be calculated through the following equations (Eqs. (9)–(12)):

$$P = A^2 + B^8 + C^{12} \quad (9)$$

$$A = \sum_{i=1}^{5} K^i \sum_{j=0}^{2} a_{ij} S^j \quad (10)$$

$$B = \sum_{i=0}^{4} K^i \sum_{j=0}^{2} b_{ij} S^j \quad (11)$$

$$C = \sum_{i=0}^{4} K^i \sum_{j=0}^{2} c_{ij} S^j \quad (12)$$

where P is pressure (MPa), K is temperature in Kelvin, and A, B, and C are respectively the density of seawater (g/cm^3), and S is salinity (g/kg). The coefficients of a_{ij}, b_{ij}, and c_{ij} are given in Table 3. The reported uncertainty of water density using the fitted equations is 0.09 kg/m^3 (Safarov et al., 2009, 2012, 2013).

Table 3
Coefficients for Eqs. (10)–(12) from Safarov et al., 2012.

aij		*bij*		*cij*	
a10	16.8260119036	b00	1780.94028549	c00	−1197.00357946
a11	−0.0141313351238	b01	−8.44625953277	c01	8.48513299409
a12	$0.247406490575 \times 10^{-3}$	b02	−0.0203022580799	c02	0
a20	−0.174551209401	b10	−23.9619103076	c10	11.7622451237
a21	$0.3336290751342 \times 10^{-4}$	b11	0.0616367739239	c11	−0.0571254359702
a22	$-0.102404029138 \times 10^{-5}$	b12	0	c12	0
a30	$0.590549251552 \times 10^{-3}$	b20	0.123588063860	c20	−0.040233852428
a31	0	b21	$-0.115367580107 \times 10^{-3}$	c21	$0.958997239703 \times 10^{-4}$
a32	0	b22	0	c22	$0.185255385513 \times 10^{-6}$
a40	$-0.843286627505 \times 10^{-6}$	b30	$-0.230808294277 \times 10^{-3}$	c30	$0.418262515254 \times 10^{-4}$
a41	0	b31	0	c31	0
a42	$0.482122273652 \times 10^{-11}$	b32	0	c32	0
a50	$0.444848916045 \times 10^{-9}$	b40	$0.142119761663 \times 10^{-6}$	c40	0
a51	$-0.346870313329 \times 10^{-13}$	b41	0	c41	0
a52	$-0.\ 534{,}550{,}469{,}142 \times 10^{-14}$	b42	$0.534482054293 \times 10^{-12}$	c42	$-0.986850131470 \times 10^{-12}$

Once the relative partitioning between boron species is calculated, the boron isotopic composition of the borate ion and boric acid species in the fluid and the four-coordinated BO_4 structure in phyllosilicate and serpentine is calculated using the following equations (Boschi et al., 2008) extrapolated by fitting data provided by Liu and Tossell (2005), where K is temperature in Kelvin (Eqs. (13)–(15)):

$$1000 \bullet ln\alpha_{III_{Fluid}-IV_{Fluid}} = 7.2087 \bullet \left(\frac{1000}{K}\right) + 2.3467 \quad (13)$$

$$1000 \bullet ln\alpha_{III_{Fluid}-IV_{Mineral}} = 13.43 \bullet \left(\frac{1000}{K}\right) + 4.7093 \quad (14)$$

$$1000 \bullet ln\alpha_{IV_{Fluid}-IV_{Mineral}} = 5.0225 \bullet \left(\frac{1000}{K}\right) + 3.1553 \quad (15)$$

Fractionation between fluid borate ion and boric acid in the low temperature <50 °C approach is fixed to a value of 1.0272 (Klochko et al., 2006; Yin et al., 2023). This is because although there is likely a temperature dependence to the fractionation factor at these temperatures it is currently poorly constrained and is unlikely to be large (Foster and Rae, 2016; Yin et al., 2023). New equilibrium serpentine-fluid fractionation factor equations, for both boric acid and borate species, are generated (Eqs. (16)–(18)) by fitting data provided by a recent theoretical study (Li et al., 2022):

$$1000 \bullet ln\alpha_{III_{Fluid}-IV_{Fluid}} = -6.17 + 12.65 \bullet \left(\frac{1000}{K}\right) - 0.92 \bullet \left(\frac{1000}{K}\right)^2 \quad (16)$$

$$1000 \bullet ln\alpha_{III_{Fluid}-IV_{Mineral}} = -9.09 + 20.57 \bullet \left(\frac{1000}{K}\right) + 1.18 \bullet \left(\frac{1000}{K}\right)^2 \quad (17)$$

$$1000 \bullet ln\alpha_{IV_{Fluid}-IV_{Mineral}} = -2.93 + 7.93 \bullet \left(\frac{1000}{K}\right) + 2.10 \bullet \left(\frac{1000}{K}\right)^2 \quad (18)$$

The boron isotopic compositions of the borate ion and boric acid species in the fluid at different pH and temperatures may be calculated using the following equations (Boschi et al., 2008; Zeebe and Wolf-Gladrow, 2001) (Eqs. (19)–(22)):

$$R_{[B(OH)_4]^-} = R_{Fluid} \bullet \left(\frac{1 + \alpha_{IV-III} 10^{pK_B - pH}}{1 + 10^{pK_B - pH}}\right) \quad (19)$$

$$R_{[B(OH)_3]} = \frac{R_{[B(OH)_4]^-}}{\alpha_{IV-III}} \quad (20)$$

$$\alpha_{IV-III} = \frac{1}{\alpha_{III-IV}} \quad (21)$$

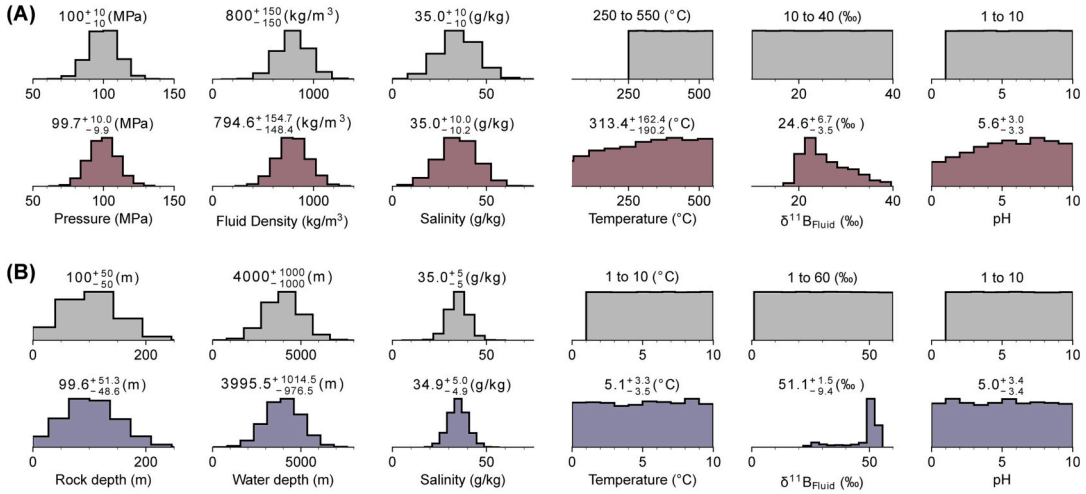

Fig. 4. Prior and posterior probability distributions from the (A) high temperature and (B) low temperature basalt-seawater exchange scenarios (Figs. 4; 6). Grey histograms denote prior probability distributions and coloured histograms denote posterior probability distributions. Median values are reported with uncertainty equivalent to 1σ.

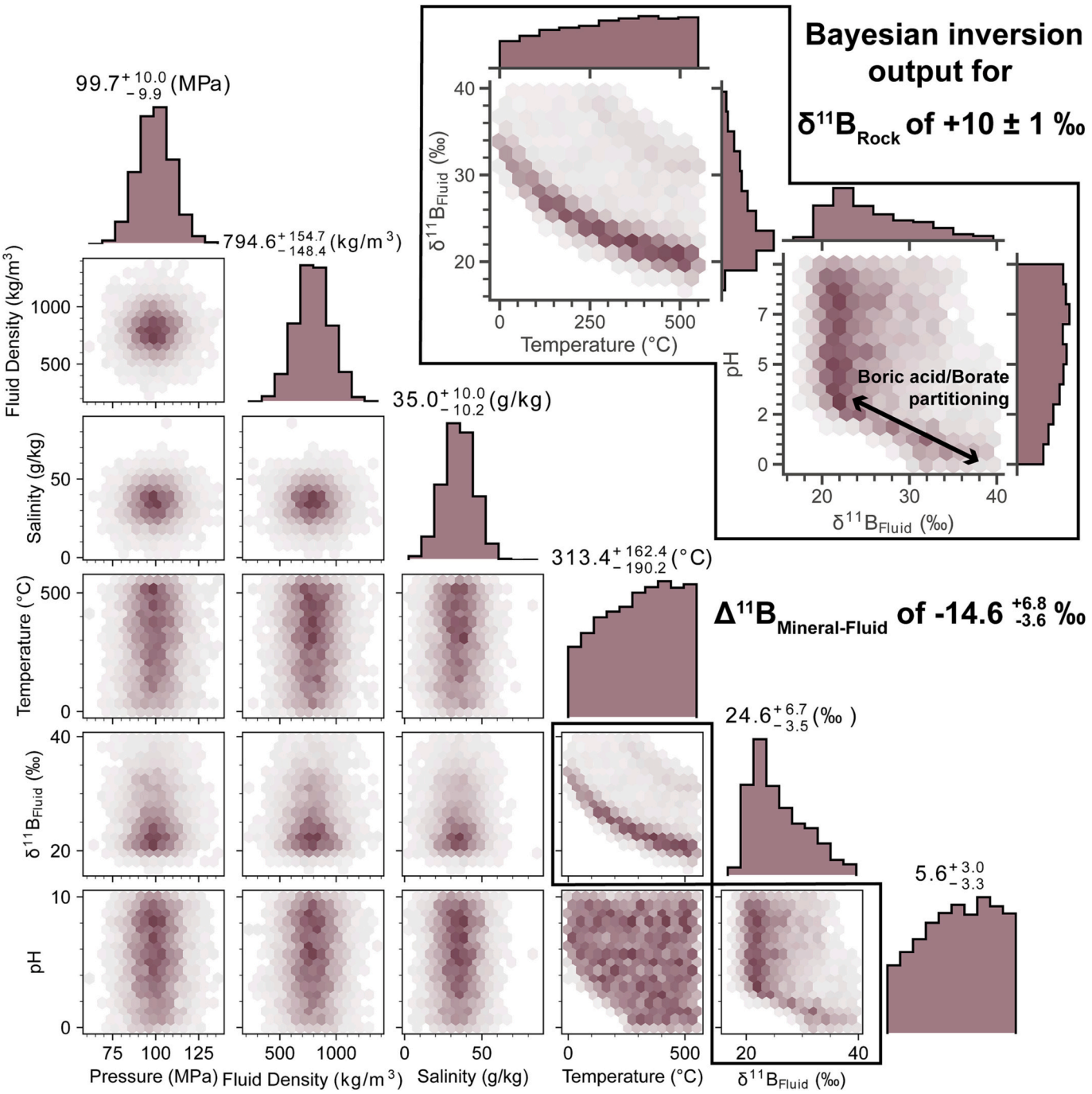

Fig. 5. Multi-dimensional EquiB posterior probability distributions are shown plotted as hexagonally binned histogram plots using a high temperature (>50 °C) regime and equations of Arcis et al., 2017. Fractionation factors are fitted based on data from Liu and Tossell, 2005. Median values are reported with uncertainty equivalent to 1σ.

$$R_{Fluid} = \left(\left(\frac{\delta^{11}B_{Fluid}}{1000}\right)+1\right) \bullet \frac{^{11}B}{^{10}B} SRM951 \quad (22)$$

The $^{11}B/^{10}B$ ratios (defined as R) are converted to $\delta^{11}B$ notation and the $\delta^{11}B$ mineral values in equilibrium with both boric acid and borate ion species in fluid are calculated using the following equations, where n is 2 (Eqs. (23)–(25)):

$$\delta^{11}B_{Mineral\ (1)} = \left(\frac{\left(1000+\delta^{11}B_{[B(OH)_3]}\right)}{\alpha_{III_{Fluid}-IV_{Mineral}}}\right) - 1000 \quad (23)$$

$$\delta^{11}B_{Mineral\ (2)} = \left(\frac{\left(1000+\delta^{11}B_{[B(OH)_4]^-}\right)}{\alpha_{IV_{Fluid}-IV_{Mineral}}}\right) - 1000 \quad (24)$$

$$\delta^{11}B_{Mineral\ (Mean)} = \frac{\sum_{i=1}^{n}\delta^{11}B_i}{n} \quad (25)$$

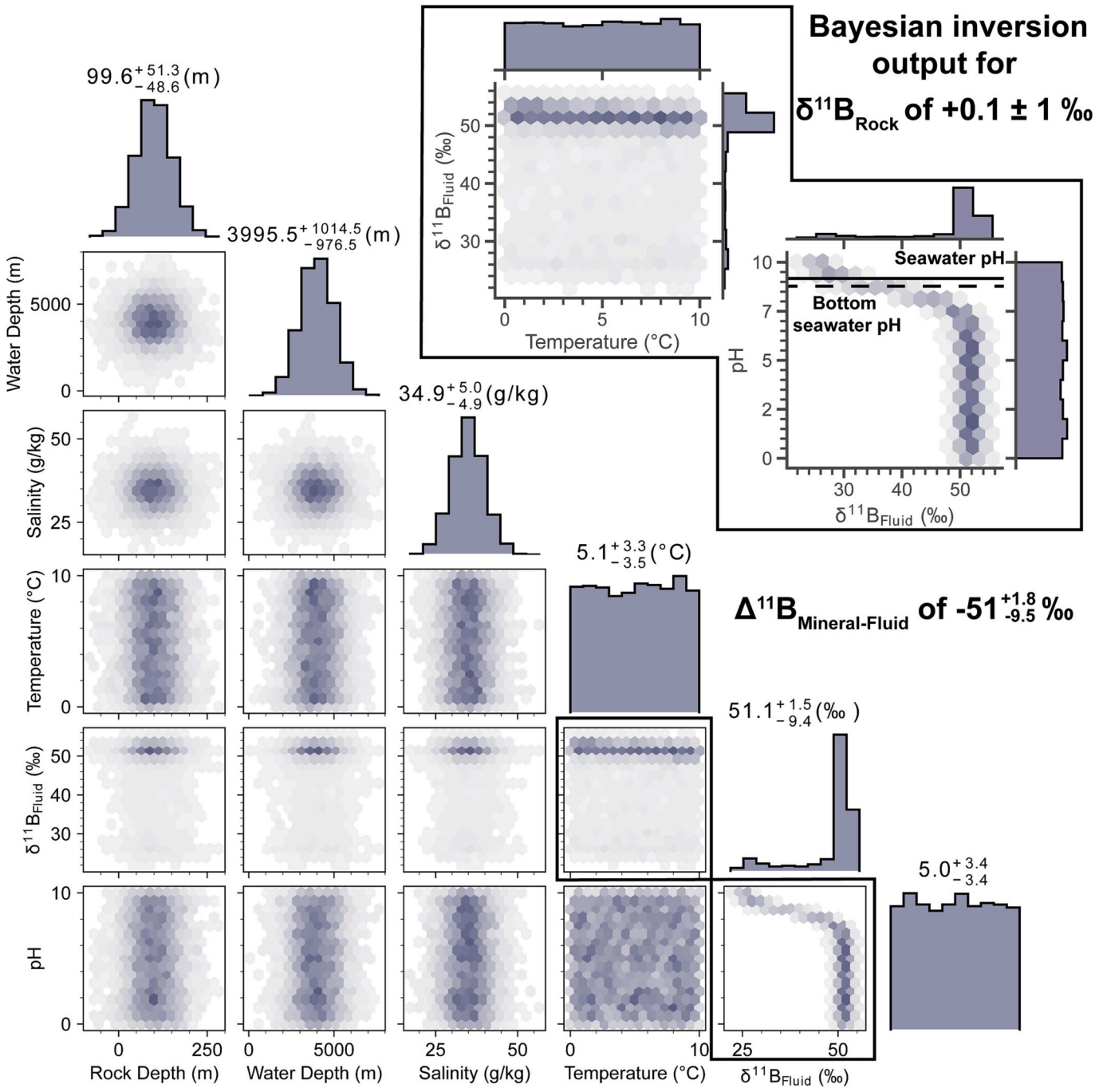

Fig. 6. Multi-dimensional EquiB posterior probability distributions are shown plotted as hexagonally binned histogram plots using a low temperature (<50 °C) regime and equations of Dickson, 1990 and Millero, 1995. Fractionation factors are fitted based on data from Liu and Tossell, 2005. Median values are reported with uncertainty equivalent to 1σ.

2.2. Bayesian inversion engine

The boron equilibrium fractionation equations described above require knowledge of multiple physical parameters including temperature, salinity, pressure, fluid density, and pH that are often poorly constrained in natural systems (e.g., Palmer, 1996). To constrain the uncertainty and the relative sensitivities of the underlying physical parameters required to calculate the $\delta^{11}B$ of a rock or mineral in equilibrium with a fluid, we combine these boron fractionation equations with a Bayesian inversion approach, which leverages the UltraNest engine (Buchner, 2014, 2017, 2021a). The term "engine" here refers to a comprehensive computational framework that executes Bayesian inference. This approach provides parameter-based constraints of the data by implementing the Monte Carlo technique Nested Sampling (Skilling, 2004) that explores parameter space by applying Bayesian inference on defined prior probability distributions and consequently generates posterior probability distributions (Fig. 4) (Buchner, 2021a). The UltraNest engine employs the MLFriends algorithm, where a fixed size of live points ($n = 1600$) are drawn randomly from prior probability distributions and are then clustered into ellipsoids (Buchner, 2021b). The shape of the ellipsoid is determined by the Mahalanobis distance and the ellipsoid size is determined by bootstrapping (Buchner, 2021a). Inside the ellipsoid, new points are sampled from the prior and the worst fitting point is removed, resulting in the live point sampled volume

shrinking by a constant factor (Buchner, 2021a, 2021b). Nested sampling iterates and records the likelihood as the sampled volume decreases. Once the remaining volume fails to contribute any probability mass, the exploration of the prior distribution is terminated and the volume of the removed points reflect the posterior samples (Buchner, 2014, 2021a, 2021b). This method provides a powerful approach in estimating the parameters of a forward model as it is theoretically justified and free of tuning parameters.

2.3. Equilibrium model assumptions and limitations

The approach outlined in this study assumes that fluid-mineral exchange occurred under equilibrium conditions and does not account for disequilibrium. The model does not account for mass transfer between respective boron reservoirs and does not employ a Rayleigh-type distillation calculation. It also does not include a tracer transport component or account for the uncertainty within individual fractionation factors nor the relatively small influence of major ion chemistry on pK_B (e.g. Hershey et al., 1986). The low temperature (0 to 45 °C; Dickson, 1990; Millero, 1995) and high temperature (25 to 350 °C; Arcis et al., 2017) approaches in determining the boron dissociation constant (pK_B) results in contrasting pK_B values (Fig. 3). At 25 °C the difference between in the pK_B values is 3.7 and at 300 °C the difference in pK_B is 0.1. In this study, we apply both approaches under different temperature

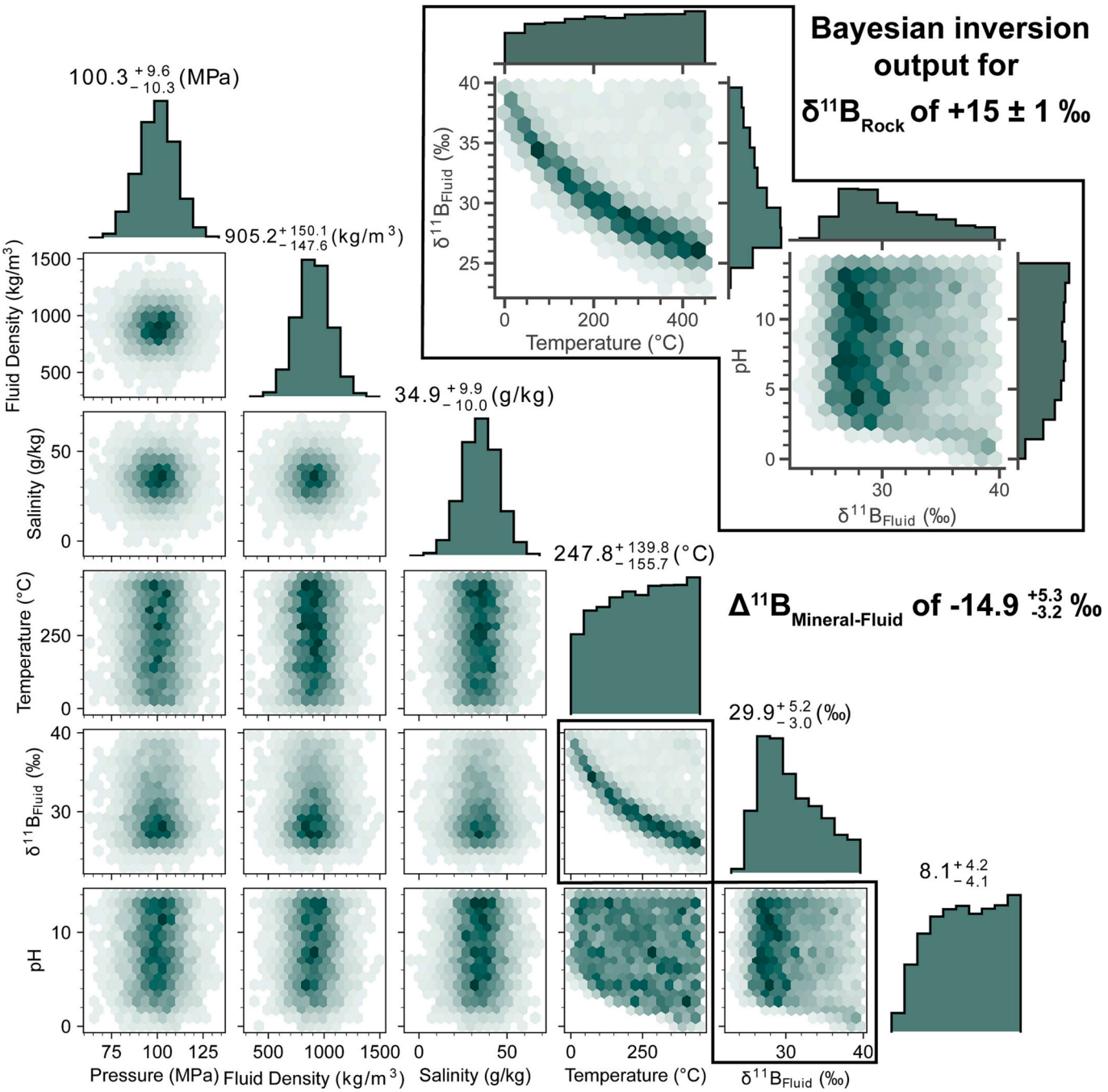

Fig. 7. Multi-dimensional EquiB posterior probability distributions are shown plotted as hexagonally binned histogram plots using a high temperature (>50 °C) regime and equations of Arcis et al., 2017. Fractionation factors are fitted based on data from Liu and Tossell, 2005. Median values are reported with uncertainty equivalent to 1σ.

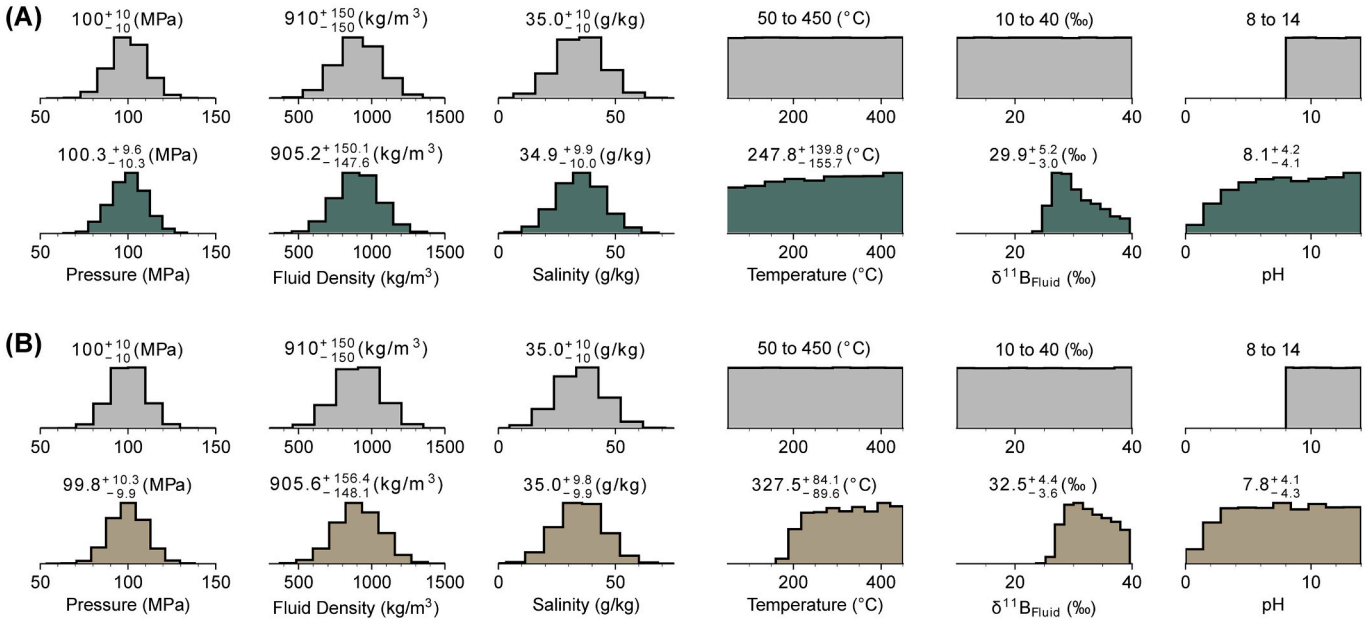

Fig. 8. Prior and posterior probability distributions from the (A) phyllosilicate-serpentine fractionation factors (Liu and Tossell, 2005) and (B) serpentine fractionation factors (Li et al., 2022) scenarios (Figs. 7; 9). Grey histograms denote prior probability distributions and coloured histograms denote posterior probability distributions. Median values are reported with uncertainty equivalent to 1σ.

regimes (Fig. 2). As the equations of Dickson (1990) are proposed for temperatures between 0 and 45 °C, we apply these equations in our low temperature (defined here as <50 °C) basalt-seawater exchange scenario. The equations of Arcis et al. (2017) are proposed for a wider temperature range (25 to 350 °C) and we apply these equations in our high temperature (defined here as >50 °C) basalt-seawater and peridotite-fluid exchange scenarios. We do not explore the transitional temperature space around 50 °C. It remains unclear whether the respective pK_B determination equations applied under different temperature regimes in this study are valid and further investigations are required to refine the experimentally derived pK_B values. Recent studies have indicated that at low temperatures (<50 °C), high concentrations of boron within the fluid phase influence fractionation due to the presence of polyborate ion species, in addition to boric acid and borate ion (Gu et al., 2023). As our low temperature approach is applied to a seawater-basalt exchange scenario and polyborate ions are likely not present, our calculations account for borate ion and boric acid only.

3. Results and discussion

To validate the approach of this study, we apply the contrasting high temperature and low temperature regimes (Fig. 2) within the boron equilibrium model, coupled with a Bayesian inversion engine, to several basalt-seawater and peridotite-fluid exchange scenarios. Application of this modelling approach provides robust and reproducible constraints on the underlying uncertainties of physical parameters required to calculate a $\delta^{11}B$ rock isotope value in equilibrium with a fluid (Fig. 2).

3.1. Basalt-fluid exchange scenarios

The high temperature (pK_B calculations at temperatures >50 °C; Figs. 4a; 5; Arcis et al., 2017) model simulations indicate that a basalt in equilibrium with hydrothermal fluid at conditions ranging between 250 and 550 °C and pressures of 100 MPa, where the majority of boron is located in phyllosilicate minerals with a $\delta^{11}B$ value of +10 ± 1 ‰, would require a $\delta^{11}B_{Fluid}$ isotope value of $+24.6^{+6.7}_{-3.5}$‰(1σ). At such conditions, pK_B is calculated using the equations of Arcis et al. (2017), producing pK_B values varying between ~1.8 and ~2.5. In contrast, the pK_B of unmodified seawater at standard T and P is typically ~8.6 (Dickson, 1990; Rae, 2018). Such low pK_B values of ~1.8 to ~2.5 reflect a fluid dominated by borate (following Arcis et al., 2017; Dickson, 1990), resulting in less pH-dependent fractionation relative to fluids dominated by boric acid (Fig. 5). Under these hydrothermal conditions, because the pK_B is the pH at which the concentrations of boric acid and borate ion are equal, if the pH of the fluid during isotopic exchange is significantly greater (or lower) than the pK_B the boron isotopic composition of the mineral is generally insensitive to pH of the fluid (Fig. 5). In addition, fluid density, pressure, and salinity also appear to have a minimal effect on $\Delta^{11}B_{Mineral\text{-}Fluid}$ (Figs. 4a; 5). In contrast, temperature and $\delta^{11}B_{Fluid}$ are negatively correlated, showing that temperature has a significant control on $\Delta^{11}B_{Mineral\text{-}Fluid}$ fractionation at the conditions presented (Fig. 5) with the model estimating a primarily temperature controlled $\Delta^{11}B_{Mineral\text{-}Fluid}$ value of $-14.6^{+6.8}_{-3.6}$‰(1σ).

Previous experimental studies proposed illite/smectite $\Delta^{11}B_{Mineral\text{-}Fluid}$ values of −16 ‰ and − 13 ‰ at 300 and 350 °C respectively at 100 MPa and pH of 6 (Williams et al., 2001). This suggests that the boron equilibrium model and Bayesian inversion engine presented here yields $\Delta^{11}B_{Mineral\text{-}Fluid}$ values consistent with experimentally derived boron fractionation factors of similar mineral types at similar conditions (Fig. 4a). In addition, the estimated $\delta^{11}B_{Fluid}$ value of $+24.6^{+6.7}_{-3.5}$‰(1σ), is consistent with previously measured boron isotopic composition of hydrothermal fluids sampled from high-temperature vent sites that range between +24.3 and +36.8 ‰ ($n = 29$; James et al., 1995; Palmer, 1991, 1996; Spivack and Edmond, 1987; You et al., 1994). As the results from the boron equilibrium model coupled with a Bayesian inversion engine yield reasonable outputs consistent with empirical studies, we propose that the modelling approach outlined above is valid to within the robustly constrained uncertainties provided.

The low temperature (<50 °C; Figs. 4b; 6; Dickson, 1990; Millero, 1995) basalt-seawater model scenario indicates that a seafloor basalt altered by seawater with a measured rock $\delta^{11}B$ isotope value of +0.1 ± 1 ‰ (e.g., Spivack and Edmond, 1987) in equilibrium with seawater, at temperatures ranging between 1 and 10 °C, would require a median $\delta^{11}B_{Fluid}$ isotope value of$+51.1^{+1.5}_{-9.4}$‰(1σ). The relationship between pH and $\delta^{11}B_{Fluid}$ shows the pH-dependent fractionation in this scenario, where values of pH >7 yield significantly lower $\delta^{11}B_{Fluid}$ compositions

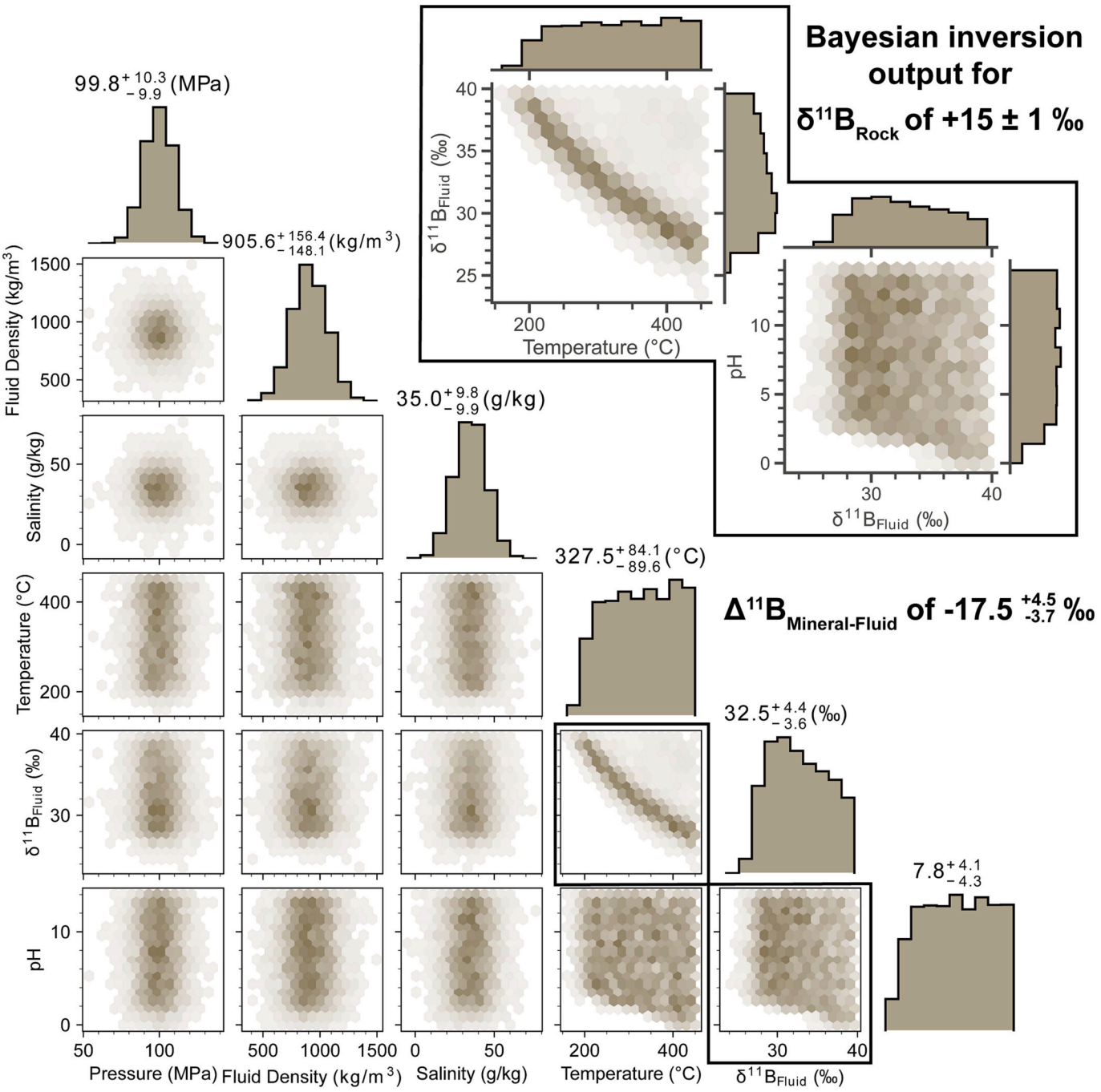

Fig. 9. Multi-dimensional EquiB posterior probability distributions are shown plotted as hexagonally binned histogram plots using a high temperature (>50 °C) regime and equations of Arcis et al., 2017. Fractionation factors are fitted based on data from Li et al., 2022. Median values are reported with uncertainty equivalent to 1σ.

(Fig. 6), resulting in a $\Delta^{11}B_{Mineral\text{-}Fluid}$ value with asymmetric uncertainty skewed towards lower $\delta^{11}B_{Fluid}$. The boron isotopic composition of seawater is +39.61 ‰ (Foster et al., 2010), indicating that equilibrium basalt-seawater boron exchange likely occurred with a modified seawater with a heavier fluid $\delta^{11}B$. Such modification is proposed to occur during low temperature seawater-boron exchange as boron is removed from seawater and sequestered into secondary mineral assemblages of altered basalts, modifying the boron isotopic composition of the altering fluid to heavier isotopic values relative to seawater (James et al., 1995; Spivack and Edmond, 1987). In contrast to the high temperature scenario, the low temperature basalt-seawater output is not consistent with previous experimentally derived equilibrium boron isotope smectite-fluid fractionation extents that yield $\Delta^{11}B_{Mineral\text{-}Fluid}$ values ranging from −34.3 ± 0.2 ‰ at 5 °C and pH of 6.65 and −23.4 ± 0.2 ‰ at 40 °C and pH of 8.45 (Palmer et al., 1987). These experimentally derived fractionation extents are significantly less than the median $\Delta^{11}B_{Mineral\text{-}Fluid}$ value of $-51^{+1.8}_{-9.5}$‰(1σ) proposed in the basalt-seawater exchange scenario presented in this study but fall within 2σ of the median value. Some of this divergence is likely related to our modelling scenario occurring over a wide pH range of $5^{+3.4}_{-3.4}$‰(1σ) and our calculations including pressure at a typical seafloor ocean depth (~4000 m) (Fig. 6). In contrast, previous investigations of $\Delta^{11}B_{Mineral\text{-}Fluid}$ fractionation at low temperatures are for discrete pH values and do not account for pressure (Palmer et al., 1987).

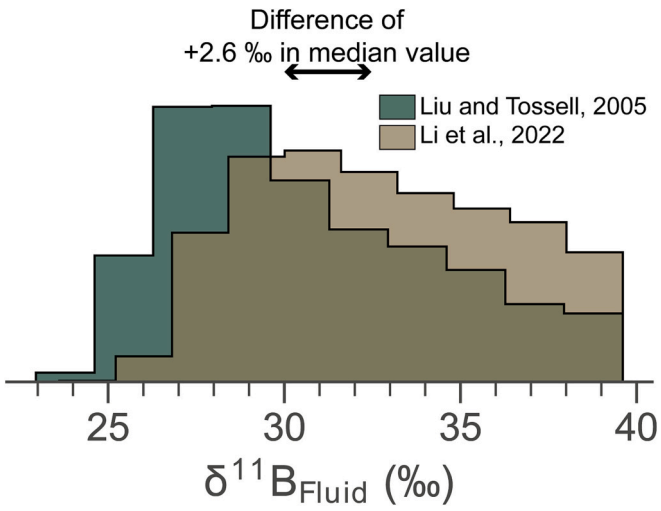

Fig. 10. EquiB posterior probability distributions of calculated $\delta^{11}B$ fluid values are shown as a histogram plot using a high temperature (>50 °C) regime and equations of Arcis et al., 2017. Prior probability distributions are outlined in Fig. 8. Fractionation factors are fitted based on data from Liu and Tossell, 2005 and Li et al., 2022.

3.2. Peridotite-fluid exchange scenarios

The model output under a peridotite-fluid exchange scenario using phyllosilicate-serpentine fractionation factors (Liu and Tossell, 2005) (Figs. 7, 8a) suggests that a serpentinite composed of serpentine polymorphs lizardite or chrysotile with a median $\delta^{11}B$ value of +15 ± 1 ‰ would be in isotopic equilibrium with a fluid of $+29.9^{+5.2}_{-3.0}$‰(1σ) at a median temperature of 248^{+140}_{-156}°C (1σ) (Fig. 8a). Application of the peridotite-fluid exchange scenario using serpentine fractionation factors (Li et al., 2022) and identical prior probability distributions (Fig. 8) suggests similar values with a fluid median $\delta^{11}B$ of $+32.5^{+4.4}_{-3.6}$‰(1σ) in isotopic equilibrium with a serpentinite of +15 ± 1 ‰ (Fig. 9). These results indicate temperature is the greatest control on the extent of serpentine-fluid fractionation (Fig. 7). Other parameters such as pressure, salinity, and fluid density exert only minimal influence on the extent of serpentine-fluid fractionation. In addition, pH-dependent fractionation has little effect on $\Delta^{11}B_{Mineral\text{-}Fluid}$ values unless the pH of the fluid is <2 (Figs. 7, 8a). In serpentinizing conditions such low pH conditions are highly unlikely as serpentinization reactions generate alkaline to hyperalkaline waters (e.g., Barnes and O'Neil, 1969). Therefore, boron speciation in the fluids of serpentinizing environments is likely dominated by borate ion over a wide range of pH from >2 to ~13 (Figs. 7, 8a).

Previous studies have proposed that a fluid dominated by borate ion produces negligible serpentine-fluid fractionation resulting in serpentinite and the serpentinizing fluid having similar boron isotopic compositions (e.g., Benton et al., 2001; Spivack and Edmond, 1987). In contrast, our results using phyllosilicate-serpentine and serpentine fractionation factors (Li et al., 2022; Liu and Tossell, 2005), suggest that in borate-dominated serpentinizing environments the extent of $\Delta^{11}B_{Mineral\text{-}Fluid}$ is $-14.9^{+5.3}_{-3.2}$‰(1σ) and $-17.5^{+4.5}_{-3.7}$‰(1σ) respectively (Figs. 7, 9).

Recent experimentally derived serpentine fractionation factors (Hansen et al., 2017) are different from ab initio calculated fractionation factors (Li et al., 2022; Liu and Tossell, 2005) and, for example, (Hansen et al., 2017) suggest $\Delta^{11}B_{Mineral\text{-}Fluid}$ values of −3.5 ‰ at 200 °C. These experimentally derived fractionation extents are significantly smaller than our results of $\Delta^{11}B_{Mineral\text{-}Fluid}$ is $-14.9^{+5.3}_{-3.2}$‰(1σ) and $-17.5^{+4.5}_{-3.7}$‰ (1σ) at temperatures of 248^{+140}_{-156}°C (1σ) and 328^{+84}_{-90}°C (1σ) respectively (Li et al., 2022; Liu and Tossell, 2005). These discrepancies may be due to the loss of boron from the serpentine mineral phase during the experimental purging procedure leading to minimal fractionation as proposed by Hansen et al. (2017).

Li et al. (2022) have also suggested that there is a significant discrepancy in calculated $\Delta^{11}B_{Mineral\text{-}Fluid}$ fractionation of ~17 ‰ at 200 °C in their theoretically derived phyllosilicate-serpentine and serpentine fractionation factors (Li et al., 2022; Liu and Tossell, 2005). However, our results suggests that the difference in the $\Delta^{11}B_{Mineral\text{-}Fluid}$ between the different sets of fractionation factors is only ~2.6 ‰ (Fig. 10). This reduction in the difference of $\Delta^{11}B_{Mineral\text{-}Fluid}$ value between the fractionation equation sets is attributed to our direct calculation of the boron dissociation constant rather than assuming the range of relative proportion (0 to 1) of fluid borate ion and boric acid (Li et al., 2022) (Fig. 10). Therefore, both theoretically derived serpentine fractionation equations (Li et al., 2022; Liu and Tossell, 2005) yield $\Delta^{11}B_{Mineral\text{-}Fluid}$ that are in closer agreement than previously reported. Consequently, either theoretically derived fractionation factor can be applied to understanding boron fluid-serpentine exchange systematics.

4. Conclusions

Our modelling approach overcomes difficulties of previous modelling attempts by robustly calculating the boron dissociation constant under different temperature regimes. These calculations show a negative correlation between temperature and $\delta^{11}B_{Fluid}$ that indicates that temperature has the greatest control on the magnitude of equilibrium boron mineral-fluid fractionation. pH-dependent fractionation also exerts a key control at low temperatures (<50 °C) but at typical hydrothermal conditions (>50 to <550 °C) pH-dependent fractionation is negligible. Consequently, at typical hydrothermal conditions pH-dependent fractionation will only occur if the pH of the fluid is ~<2, which is unlikely in serpentinizing environments. Thus, the boron speciation of serpentinizing fluids are likely dominated by the borate ion. Other parameters such as fluid density, pressure, and salinity have little effect on the extent of boron mineral-fluid fractionation at geologically reasonable conditions.

Model outputs are in agreement with experimentally derived fractionation factors at typical hydrothermal conditions (>50 °C), but there is divergence between experimental and theoretical fractionation estimates at lower temperatures (<50 °C). Our results also suggest that the difference in previously reported $\Delta^{11}B_{Mineral\text{-}Fluid}$ values attributed to theoretically calculated phyllosilicate-serpentine and serpentine fractionation equations are much lower than previously stated with a difference of only ~2.6 ‰ in the calculated median value. Our preference is for these theoretically derived fractionation equations. In contrast, experimentally determined pK_B values show significant differences at 25 °C with theoretical values although there is convergence at ~300 °C. Further investigations are required to understand why the differing approaches form distinct trends rather than a continuum of pK_B values.

In summary, the development of a robust and reproducible boron equilibrium model, named here EquiB, coupled with a Bayesian inversion engine yields a deeper knowledge of boron systematics. The approach outlined constrains the underlying uncertainty of physical parameters encoded into a boron isotopic composition of a rock in equilibrium with a fluid. The provided constraints of underlying uncertainty enable meaningful interpretation of boron isotope analyses and greater confidence in our ability to fingerprint isotopic compositions. As new constraints emerge the EquiB framework can be updated easily. Our approach is not limited to hydrothermal alteration and serpentinization environments, and with necessary modifications, EquiB could be expanded and applied to other mineral systems.

CRediT authorship contribution statement

Aled D. Evans: Conceptualization, Data curation, Formal analysis, Funding acquisition, Investigation, Methodology, Project

administration, Software, Validation, Visualization, Writing – original draft, Writing – review & editing. **Gavin L. Foster:** Investigation, Supervision, Validation, Writing – review & editing. **Damon A.H. Teagle:** Supervision, Writing – review & editing, Investigation, Validation, Funding acquisition.

Declaration of competing interest

The authors declare that they have no known competing financial interests or personal relationships that could have appeared to influence the work reported in this paper.

Data availability

EquiB code is supplied in the supplementary materials.

Acknowledgements

Aled D. Evans acknowledges a Natural Environmental Research Council–SPITFIRE CASE PhD award NE/L002531/1 (Natural History Museum CASE partner). We thank Martin Palmer for his comments on this manuscript. We thank Michael Böttcher for editorial handling and two anonymous reviewers for their constructive reviews.

Appendix A. Supplementary data

Supplementary data to this article can be found online at https://doi.org/10.1016/j.chemgeo.2024.121953.

References

Arcis, H., Ferguson, J.P., Applegarth, L., Zimmerman, G.H., Tremaine, P.R., 2017. Ionization of boric acid in water from 298 K to 623 K by AC conductivity and Raman spectroscopy. J. Chem. Thermodyn. 106, 187–198.
Barnes, I., O'Neil, J.R., 1969. The relationship between fluids in some fresh alpine-type ultramafics and possible modern serpentinization, Western United States. GSA Bull. 80, 1947–1960.
Barth, S., 1998. Application of boron isotopes for tracing sources of anthropogenic contamination in groundwater. Water Res. 32, 685–690.
Benton, L.D., Ryan, J.G., Tera, F., 2001. Boron isotope systematics of slab fluids as inferred from a serpentine seamount, Mariana forearc. Earth Planet. Sci. Lett. 187, 273–282.
Boschi, C., Dini, A., Früh-Green, G.L., Kelley, D.S., 2008. Isotopic and element exchange during serpentinization and metasomatism at the Atlantis Massif (MAR 30°N): insights from B and Sr isotope data. Geochim. Cosmochim. Acta 72, 1801–1823.
Buchner, J., 2014. A Statistical Test for Nested Sampling Algorithms. arXiv [stat.CO].
Buchner, J., 2017. Collaborative Nested Sampling: Big Data vs. Complex Physical Models. arXiv [stat.CO].
Buchner, J., 2021a. UltraNest – A Robust, General Purpose Bayesian Inference Engine. arXiv [stat.CO].
Buchner, J., 2021b. Nested Sampling Methods. arXiv [stat.CO].
Catanzaro, E.J., 1970. Boric Acid: Isotopic and Assay Standard Reference Materials. National Bureau of Standards, Institute for Materials Research.
Craig, H., 1961. Isotopic variations in meteoric waters. Science 133, 1702–1703.
Deyhle, A., Kopf, A.J., 2005. The use and usefulness of boron isotopes in natural silicate–water systems. Phys. Chem. Earth A/B/C 30, 1038–1046.
Dickson, A.G., 1990. Thermodynamics of the dissociation of boric acid in synthetic seawater from 273.15 to 318.15 K. Deep Sea Res. A 37, 755–766.
Foster, G.L., Rae, J.W.B., 2016. Reconstructing ocean pH with boron isotopes in foraminifera. Annu. Rev. Earth Planet. https://doi.org/10.1146/annurev-earth-060115-012226.
Foster, G.L., Lécuyer, C., Marschall, H.R., 2016. Boron Stable Isotopes. In: Encyclopedia of Earth Sciences Series, Encyclopedia of Earth Sciences. Springer International Publishing, Cham, pp. 1–6.
Foster, G.L., Pogge von Strandmann, P.A.E., Rae, J.W.B., 2010. Boron and magnesium isotopic composition of seawater. Geochem. Geophys. Geosyst. 11 https://doi.org/10.1029/2010gc003201.
Gu, H., Ma, Y., Peng, Z., Zhu, F., Ma, X., 2023. Influence of polyborate ions on the fractionation of B isotopes during calcite deposition. Chem. Geol. 622, 121387.
Hansen, C.T., Meixner, A., Kasemann, S.A., Bach, W., 2017. New insight on Li and B isotope fractionation during serpentinization derived from batch reaction investigations. Geochim. Cosmochim. Acta 217, 51–79.
Harkness, J.S., Warner, N.R., Ulrich, A., Millot, R., Kloppmann, W., Ahad, J.M.E., Savard, M.M., Gammon, P., Vengosh, A., 2018. Characterization of the boron, lithium, and strontium isotopic variations of oil sands process-affected water in Alberta, Canada. Appl. Geochem. 90, 50–62.
Hershey, J.P., Fernandez, M., Milne, P.J., Millero, F.J., 1986. The ionization of boric acid in NaCl, Na-Ca-Cl and Na-Mg-Cl solutions at 25°C. Geochim. Cosmochim. Acta 50, 143–148.
James, R.H., Palmer, M.R., 2000. Marine geochemical cycles of the alkali elements and boron: the role of sediments. Geochim. Cosmochim. Acta 64, 3111–3122.
James, R.H., Elderfield, H., Palmer, M.R., 1995. The chemistry of hydrothermal fluids from the Broken Spur site, 29°N Mid-Atlantic ridge. Geochim. Cosmochim. Acta 59, 651–659.
Kakihana, H., Kotaka, M., Satoh, S., Nomura, M., Okamoto, M., 1977. Fundamental studies on the ion-exchange separation of boron isotopes. BCSJ 50, 158–163.
Klochko, K., Kaufman, A.J., Yao, W., Byrne, R.H., Tossell, J.A., 2006. Experimental measurement of boron isotope fractionation in seawater. Earth Planet. Sci. Lett. 248, 276–285.
Knudsen, M., 1901. Hydrographische Tabellen. GEC Gad.
Kowalski, P.M., Wunder, B., 2018. Boron isotope fractionation among vapor–liquids–solids–melts: experiments and atomistic modeling. In: Marschall, H., Foster, G. (Eds.), Boron Isotopes: The Fifth Element. Springer International Publishing, Cham, pp. 33–69.
Lemarchand, D., Gaillardet, J., Lewin, E., Allègre, C.J., 2000. The influence of rivers on marine boron isotopes and implications for reconstructing past ocean pH. Nature 408, 951–954.
Li, Y.-C., Wei, H.-Z., Palmer, M.R., Ma, J., Jiang, S.-Y., Chen, Y.-X., Lu, J.-J., Liu, X., 2022. Equilibrium boron isotope fractionation during serpentinization and applications in understanding subduction zone processes. Chem. Geol. 609, 121047.
Liu, Y., Tossell, J.A., 2005. Ab initio molecular orbital calculations for boron isotope fractionations on boric acids and borates. Geochim. Cosmochim. Acta 69, 3995–4006.
Martin, C., Flores, K.E., Harlow, G.E., 2016. Boron isotopic discrimination for subduction-related serpentinites. Geology 44. https://doi.org/10.1130/G38102.1.
Millero, F.J., 1995. Thermodynamics of the carbon dioxide system in the oceans. Geochim. Cosmochim. Acta 59, 661–677.
Millero, F.J., 2010. History of the equation of state of seawater. Oceanography 23, 18–33.
Nir, O., Vengosh, A., Harkness, J.S., Dwyer, G.S., Lahav, O., 2015. Direct measurement of the boron isotope fractionation factor: reducing the uncertainty in reconstructing ocean paleo-pH. Earth Planet. Sci. Lett. 414, 1–5.
Palmer, M.R., 1991. Boron isotope systematics of hydrothermal fluids and tourmalines: a synthesis. Chem. Geol. 94, 111–121.
Palmer, M.R., 1996. Hydration and uplift of the oceanic crust on the Mid-Atlantic Ridge associated with hydrothermal activity: evidence from boron isotopes. Geophys. Res. Lett. 23, 3479–3482.
Palmer, M.R., Spivack, A.J., Edmond, J.M., 1987. Temperature and pH controls over isotopic fractionation during adsorption of boron on marine clay. Geochim. Cosmochim. Acta 51, 2319–2323.
Rae, J.W.B., 2018. Boron isotopes in foraminifera: systematics, biomineralisation, and CO2 reconstruction. In: Marschall, H., Foster, G. (Eds.), Boron Isotopes: The Fifth Element. Springer International Publishing, Cham, pp. 107–143.
Safarov, J., Millero, F., Feistel, R., Heintz, A., Hassel, E., 2009. Thermodynamic properties of standard seawater: extensions to high temperatures and pressures. Ocean Sci. 5, 235–246.
Safarov, J., Berndt, S., Millero, F., Feistel, R., Heintz, A., Hassel, E., 2012. (p,ρ,T) properties of seawater: extensions to high salinities. Deep-Sea Res. I Oceanogr. Res. Pap. 65, 146–156.
Safarov, J., Berndt, S., Millero, F.J., Feistel, R., Heintz, A., Hassel, E.P., 2013. (p,ρ,T) properties of seawater at brackish salinities: extensions to high temperatures and pressures. Deep-Sea Res. I Oceanogr. Res. Pap. 78, 95–101.
Skilling, J., 2004. Nested sampling. AIP Conf. Proc. 735, 395–405.
Smith, H.J., Spivack, A.J., Staudigel, H., Hart, S.R., 1995. The boron isotopic composition of altered oceanic crust. Chem. Geol. 126, 119–135.
Spivack, A.J., Edmond, J.M., 1987. Boron isotope exchange between seawater and the oceanic crust. Geochim. Cosmochim. Acta 51, 1033–1043.
Vengosh, A., 1998. The isotopic composition of anthropogenic boron and its potential impact on the environment. Biol. Trace Elem. Res. 66, 145–151.
Vengosh, A., Heumann, K.G., Juraske, S., Kasher, R., 1994. Boron isotope application for tracing sources of contamination in groundwater. Environ. Sci. Technol. 28, 1968–1974.
Vengosh, A., Spivack, A.J., Artzi, Y., 1999. Geochemical and boron, strontium, and oxygen isotopic constraints on the origin of the salinity in groundwater from the Mediterranean coast of Israel. Water Resour. Res. 35, 1877–1894.
Vils, F., Tonarini, S., Kalt, A., Seitz, H.-M., 2009. Boron, lithium and strontium isotopes as tracers of seawater–serpentinite interaction at Mid-Atlantic ridge, ODP Leg 209. Earth Planet. Sci. Lett. 286, 414–425.

Williams, L.B., Hervig, R.L., Holloway, J.R., Hutcheon, I., 2001. Boron isotope geochemistry during diagenesis. Part I. Experimental determination of fractionation during illitization of smectite. Geochim. Cosmochim. Acta 65, 1769–1782.
Wunder, B., Meixner, A., Romer, R.L., Wirth, R., Heinrich, W., 2005. The geochemical cycle of boron: constraints from boron isotope partitioning experiments between mica and fluid. Lithos 84, 206–216.
Yin, X., Liu, F., Liu, Q., Zhang, Y., Gao, C., Zhang, S., Ridley, M.K., Liu, Y., 2023. Boron isotope fractionation between B(OH)3 and B(OH)4− in aqueous solution: A theoretical investigation beyond the harmonic and Born−Oppenheimer approximations. Chem. Geol. 627, 121455.
You, C.-F., Butterfield, D.A., Spivack, A.J., Gieskes, J.M., Gamo, T., Campbell, A.J., 1994. Boron and halide systematics in submarine hydrothermal systems: effects of phase separation and sedimentary contributions. Earth Planet. Sci. Lett. 123, 227–238.
Zeebe, R.E., Wolf-Gladrow, D., 2001. CO_2 in Seawater: Equilibrium, Kinetics, Isotopes. Gulf Professional Publishing.